CHALLENGE JOURNAL OF CONCRETE RESEARCH LETTERS 8 (2) (2017) 48–64

Structural behaviour of ferrocement channels slabs for low cost housing

Yousry B. I. Shaheen [a,*], Essam A. Eltehawy [b]

[a] *Department of Civil Engineering, Menoufia University, Shebin ElKoum, Menofia, Egypt*
[b] *Department of Civil Engineering, Military Technical College, Cairo, Egypt*

ABSTRACT

This paper presents a new pre cast U-shape ferrocement forms reinforced with various types of metallic and non-metallic mesh reinforcement. This research was designed to investigate the feasibility and effectiveness of employing various types of reinforcing meshes in the construction of structural slabs incorporating permanent U-shape ferrocement forms as a viable alternative for conventional reinforced concrete slabs. Fiber glass meshes reinforcement was used for durability and protection against corrosion of reinforcing steel. To accomplish this objective, an experimental program was conducted. The experimental program comprised casting and testing ten slabs having the total dimensions of 500x100x2500 mm incorporating 40 mm thick U-shape permanent ferrocement forms. Series A consists of two conventionally reinforced concrete slabs were cast and tested and used as control slab without fibers and with fibers, volume fraction, 2.05 % and 2.177 %. Series B comprises of two slabs reinforced with one and two layers of expanded steel mesh, volume fraction 2.09 and 2.42% respectively. Series C comprises two slabs reinforced with two and four layers of welded galvanized steel mesh, having volume fraction 2.05 and 2.189% respectively. Series D Consists of two slabs reinforced with one layer and two layers of fiber glass meshes, having volume fraction 2.107 and 2.277% respectively. Series E comprises two slabs reinforced with 2 layers expanded steel mesh and one layer expanded steel mesh, having volume fraction 1.357 and 2.750 % respectively. The test specimens were tested as simple slabs under four-line loadings condition on a span of 2300mm. The performance of the test slabs in terms of strength, stiffness, strains, cracking behavior, ductility, and energy absorption properties was investigated. The behavior of the developed slabs was compared to that of the control slabs. The experimental results showed that high ultimate and serviceability loads, better crack resistance control, high ductility, and good energy absorption properties could be achieved by using the proposed slabs and low cost compared with control specimen.

ARTICLE INFO

Article history:
Received 7 March 2017
Accepted 15 May 2017

Keywords:
Ferrocement channels
Deformation characteristics
Serviceability load
Cracking behaviour
Ductility
Energy absorption

1. Introduction

Recently, ferrocement has emerged as new construction material. ACI defines ferrocement as follows: "Ferrocement is a type of reinforced concrete commonly constructed of hydraulic cement mortar reinforced with closely spaced layers of relatively small wire diameter mesh. The mesh may be made of metallic or other suitable materials. The fineness of the mortar matrix and its composition should be compatible with the opening and tightness of the reinforcing system it is meant to encapsulate. The matrix may contain discontinuous fibres (Naaman and Shah, 1971; ElMohimen, 2005).

1945 Nervi built the 165 ton Motor Yatch "Prune" on a supporting frame of 6.35 mm dia. rods spaced 106 mm apart with 4 layers of wire mesh on each side of rods with total thickness of 35 mm. It weighed 5% less than a comparable wooden hull & cost 40% less at that time.

* *Corresponding author*. Tel.: +020-128-2643204 ; E-mail address: ybishaheen@yahoo.com (Y. B. I. Shaheen)
ISSN: 2548-0928 / DOI: https://doi.org/10.20528/cjcrl.2017.02.002

The first ferrocement structure - a vaulted roof over shopping centre was built in Leningrad in Soviet Union In 1974, the American Concrete Institute formed committee 549 on ferrocement. In 1975, two ferrocement aqueducts were designed & built for rural irrigation in China (Channi, 2009).

Ferrocement is now recognized as a construction material with excellent qualities of crack control, impact resistance, and toughness, largely due to the close spacing and uniform dispersion of reinforcement within the material. Many investigations have clarified the physical and mechanical properties of this material, and numerous test data are available to define its performance criteria for design and construction (Rajagoplan and Parameswaran, 1975; Singh et al., 1986; Mansur and Paramasivam, 1990; Ramesht and Vickridge, 1996; Fahmy et al., 1997a, 1997b, 2004; Wrigley, 2001; El-Sakhawy, 2007).

Structural applications of ferrocement, boats, service evaluation of ferrocement boats, tanks, silos, roofs, ferrocement as a construction material, ferrocement for repair and strengthening of structures (Naaman and Shah, 1971; Sutherland, 1972; Swamy and Abboud, 1988; Fahmy and Shaheen, 1991; Fahmy et. al., 1995, 1997a, 1997b, 1999; El-Halfawy, 2003; Ayoub, 2005; Tomar, 2006).

The successful usage of ferrocement in repairing and construction of reinforced concrete beams and the high cost of traditional wooden or steel form work led to the idea of using ferrocement laminate as permanent forms in concrete construction (Rosenthal and Bljuger, 1985; Rao and Rao, 1987; Swamy and Abboud, 1988; Abdul Kadir and Jafaar, 1993; Mays and Barnes, 1995; Abdul Kadir et. al. 1997; ACI 549-1R-88, 1998; Wrigley, 2001; Housing and Building Research Center, 2001; El-Halfawy, 2003; Abdel Tawab, 2006).

Abdul Kadir and Jaafar (1993) offered a proposed technique for using ferrocement concept to produce in situ permanent formwork as a viable alternative of traditionally used wooden forms. Ferrocement permanent formwork has great potentials in reducing construction time especially for curved structures, saving timber, and minimizing cost. It also reduces the tensile steel as a result of utilizing steel mesh which contributes also the flexural strength of the beams.

Mays and Barnes (1995) presented the results of an experimental investigation the feasibility of using pre cast ferrocement as a low permeability cover layer to the subsequently poured in situ reinforced concrete members located in environments, where there is a high risk of reinforcement corrosion. The research focused particularly on achieving an adequate and durable bond between the ferrocement layer and the concrete core in order to develop composite structural behaviour. They concluded that not only the resistance to chloride penetration was enhanced by using Styrene Butadiene Rubber (SBR) or acrylic bond coat between the ferrocement forms and the concrete, but also the use of permanent ferrocement formwork provided an increase in strength of 15% over the conventional reinforced concrete.

Abdul Kadir et al. (1997) presented the results of test on the flexural behaviour of reinforced concrete beams with ferrocement permanent formwork. One contained eight beams without mechanical shear connection between the ferrocement forms and the concrete core. And the other contained eight beams in which shear connectors shaped as 12mm × 22mm rectangular humps were placed at every 22mm centres. The area of the steel mesh was maintained constant at 55mm^2 for all beams while the area of reinforcing bars in the concrete core was variable. The results showed that the reinforced concrete beams with ferrocement permanent formwork failed by flexure under two point load test. The beams incorporating ferrocement formwork contributed from 16 to 75% to the flexural strength of the composite beams depending on steel area and the use of shear connectors. The ferrocement forms incorporating reinforced concrete core with shear connectors achieved higher strength by an average of 10% compared to the ones without shear connectors; however, they showed lower deflections when subjected to the same load.

Housing demand is rising because of the increasing population, but the high construction cost is important factor in the development of building industry. In order to balance the demand and cost for viable development of building industry, new building materials and methodology has to be developed. Ferrocement has the potential to solve many problems, technical and economic. In the construction of different types of housing systems. Housing shortages have become a dramatic fact of life in the world today. As housing demand and cost of construction both increase. Ferrocement is an excellent material for use in housing construction mainly for roofing because of its relatively low cost, durability and weather resistance. Particularly the versatility of the material further increase its utility for producing components required in housing. A ferrocement shell roof is a good example of its use in housing because of its water tightness. Unlike most conventional materials, ferrocement can be easily shaped into domes, vaults, and extruded type shapes, flat surfaces. It can span long distance and thus reduce the need for closely supports. Prefabricated ferrocement roofing elements can be produced in very interesting architectural shapes either at a factory or in site to provide relatively light roofing structures for low cost houses. The use of precast ferrocement dome and shell roofing components should be encouraged. However, attention must be given to proper detailing of joints between the roofing elements to avoid problem of water leakage through the joints.

Abdel Tawab (2006) presented the results of an investigation aiming at the development of U-shaped ferrocement permanent forms to be used for construction of reinforced concrete beams as a viable alternative to traditionally used wooden and metal formwork. The test parameters were the type of steel mesh, number of steel mesh layers. The performance of the test beams in terms of: strength, stiffness, cracking behaviour, ductility, and energy absorption properties was investigated. The results showed that high ultimate and serviceability loads, crack resistance control, high ductility, and good energy absorption properties could be achieved by using the proposed permanent ferrocement forms.

2. Experimental Program

The experimental program was divided into two phases, the first phase regarding the reinforcement; the main objective was to determine the mechanical properties of the used steel and wire meshes. The second phase, the main objective was studying the ultimate load, flexural behaviour, ductility ratio, energy absorption and mode of failure at collapse of the control slabs, which were reinforced with steel bars and u shape steel stirrups and to compare their behaviour with those reinforced ferrocement slabs reinforced with expanded metal mesh and welded galvanized steel mesh and glass fibre mesh. Skeletal steel bars and steel stirrups were used with steel meshes and fiber glass mesh. Table 1 presents details of experimental program.

In this program, ten specimens were cast and tested in order to study their behaviour under flexural loadings. Table 1 shows details of the experimental program of all the test specimens while Fig. 1 emphasizes the types of meshes and polypropylene fibers used. Fig. 2 shows reinforcement configurations details of all U shape control slabs and ferrocement channels. Fig. 3 shows photos of reinforcement configurations of all U shape slabs.

Table 1. Details of experimental program.

Series Designation	Slab No.	Volume fraction of reinforcement, %	Reinforcement details			
			Tension Steel bars, Ø 10 mm	Compression Steel bars, Ø 6 mm	No. of Stirrups, Ø 6 mm	No. and Type of Mesh Layers
A	1	2.05	4	2	15	------
	2	2.177	4	2	15	------
B	3	2.09	4	2	2	1 Layer Expanded Steel Mesh
	4	2.42	4	2	--	2 Layers Expanded Steel Mesh
C	5	2.05	4	2	4	2 Layers Welded Steel Mesh
	6	2.189	4	2	2	4 Layers Welded Steel Mesh
D	7	2.017	4	2	4	1 Layer Fibre Glass Mesh
	8	2.277	4	2	4	2 Layers Fibre Glass Mesh
E	9	1.357	--	2	--	2 Layers Expanded Steel Mesh
	10	2.750	6	2	--	1 Layer Expanded Steel Mesh

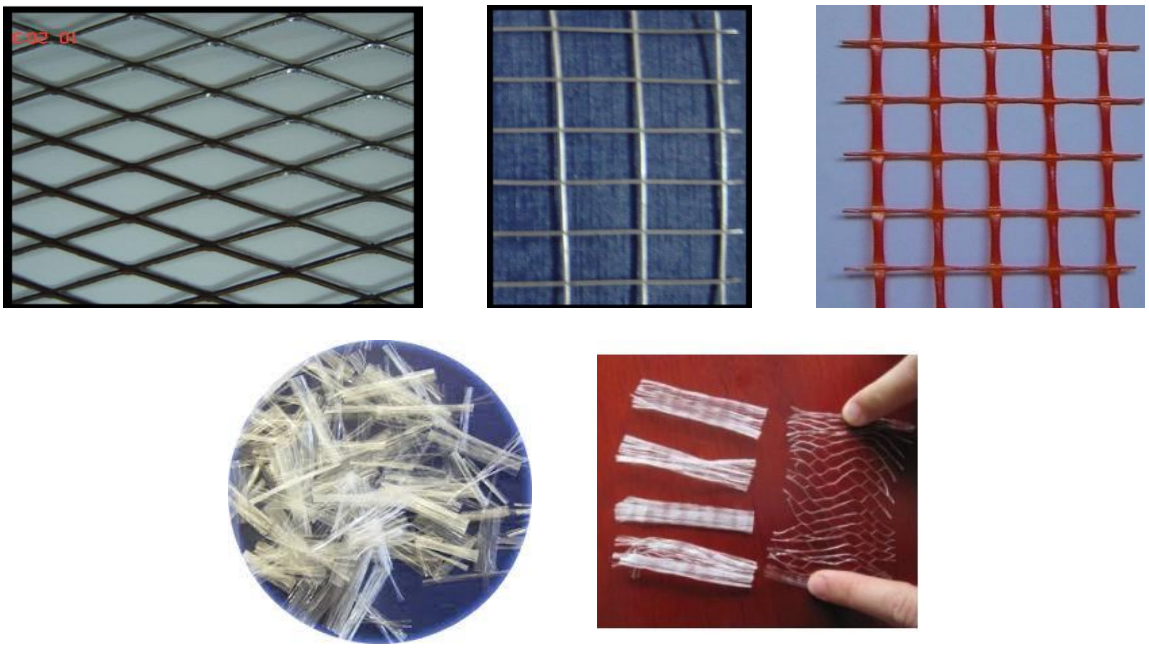

Fig. 1. Types of meshes and fibres used.

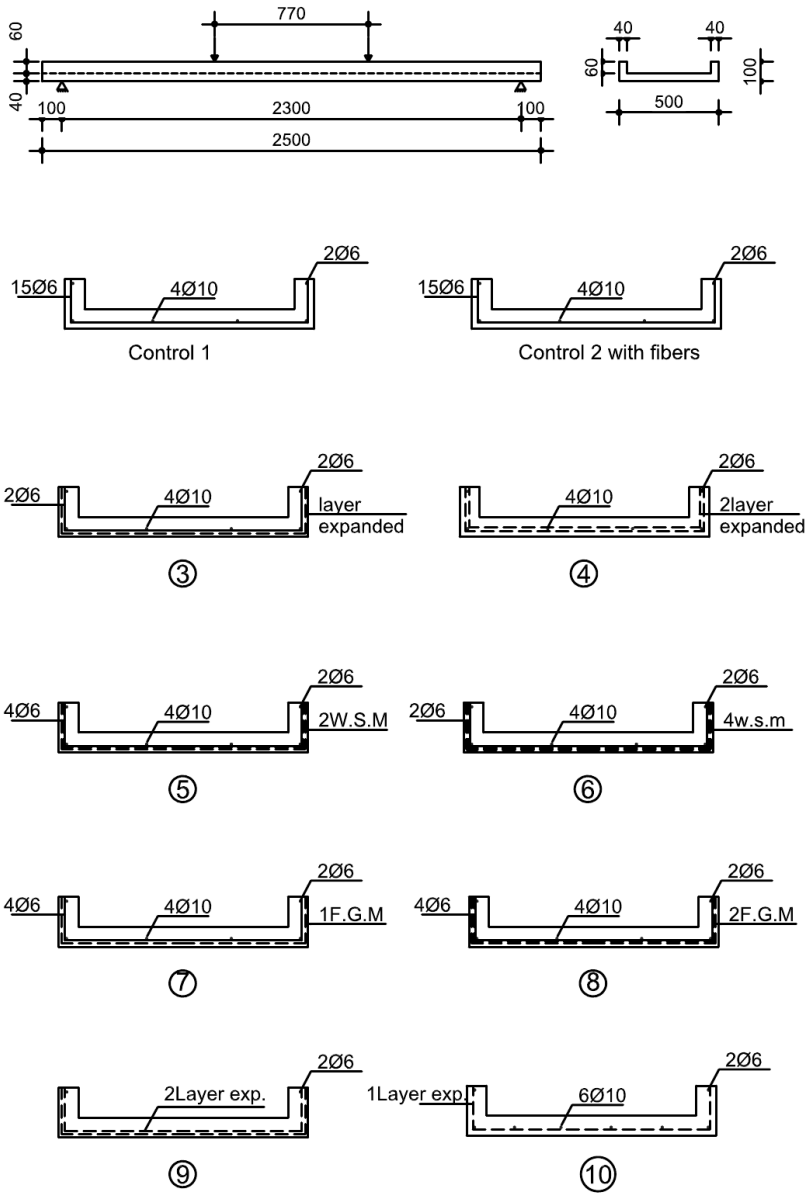

Fig. 2. Reinforcement details of all slabs.

2.1. Materials

- **The fine aggregate** used in the experimental program was of natural siliceous sand. Its characteristics satisfy the E.C.P. 203/2007 (Swamy et al, 1988) and E.S.S. 1109/2008 (Sandowicz et al., 1985). It was clean and nearly free from impurities with a specific gravity 2.6 t/m^3 and a modulus of fineness 2.7.
- **The cement** used was the Ordinary Portland cement, type produced by the Suez cement factory. Its chemical and physical characteristics satisfied the Egyptian Standard Specification E.S.S. 4657-1/2009 (Ayoub, 2005).
- **The water** used was the clean drinking fresh water free from impurities used for mixing and curing the R.C. beams tested according to the E.C.P. 203/2007 (Swamy et al., 1988).
- **Super plasticizer** used was a high rang water reducer HRWR. It was used to improve the workability of the mix. The admixture used was produced by CMB GROUP under the commercial name of Addicrete BVF. It meets the requirements of ASTM C494 (type A and F) (Singh et al., 1986). The admixture is a brown liquid having a density of 1.18 kg/litre at room temperature. The amount of HRWR was 1.0% of the cement weight.
- **Reinforcing steel**; Normal mild steel bars were used, produced from the Ezz Al Dekhila Steel - Alexandria Its chemical and physical characteristics satisfy the Egyptian Standard Specification E.S.S. 262/2011 (Sutherland, 1972). Mild steel bars of 6 mm diameter were used for stirrups with yield strength of 240 MPa.
- **Reinforcing meshes**

– **Expanded metal mesh**: Expanded metal mesh was used as reinforcement for ferrocement channels. The technical specifications and mechanical properties of expanded metal mesh as provided by producing company are given in Table 2. Fig. 1 illustrates the photo of the expanded metal mesh.

– **Welded metal mesh**: Galvanized welded metal mesh used was obtained from China. Welded metal mesh was used as reinforcement for ferrocement channels. The

technical specifications and mechanical properties of welded metal mesh as provided by producing company are given in Table 2. Fig. 1 illustrates the image.

– **Fibreglass mesh**: Fibreglass mesh used was obtained from Gavazzi Company, Italy, It was available in the Egyptian markets, The technical specifications and mechanical properties of Fibreglass mesh as provided by producing company are given in Table 2. Fig. 1 illustrates the image.

• **Polypropylene fibres** PP 300-e3 was used. It was available in the Egyptian markets. It was used in concrete mixes to produce fibrous concrete jacket to improve the concrete characteristics. The percentage of addition was chosen as 900 gm/m^3 based on the recommendations of manufacture. The technical specifications and mechanical properties of Polypropylene fibres PP 300-e3 as provided by producing company are given in Table 3. Fig. 1 illustrates the image.

Fig. 3. Reinforcement configuration of U shape slabs.

2.2. Mortar matrix

The concrete mortar used for casting channels was designed to get an ultimate compressive strength at 28-days age of (350 kg/cm^2), 35 MPa. The mix properties for mortar matrix were chosen based on the ACI Committee 549 Report (1988). For all mixes, mechanical mixer in the laboratory used mechanical mixing with capacity of 0.05 m^3, where the volume of the mixed materials was found to be within this range.

The constituent materials were first dry mixed; the mix water was added and the whole patch was re-mixed again in the mixer. The mechanical compaction was applied for all specimens. Mix proportions by weight for the different groups are given below in Table 4. Fig. 1 emphasizes the types of meshes used. Fig. 2 shows reinforcement details and photos of all control and ferrocement channels.

Table 2. Technical specifications and mechanical properties of expanded metal mesh and welded metal mesh.

Expanded Metal Mesh		Welded Metal Mesh		Fibreglass Mesh		
Style	1532	Dimensions Size	12.5×12.5 mm	Dimensions Size	12.5×11.5 mm	
Sheet Size	1×10 m	Weight	430 g/m^2	Dimensions of Strings	Longitudinal	1.66×0.66 mm
Weight	1.3 kg/m^2	Proof Stress	400 N/mm^2		Transverse	1×0.5 mm
Diamond Size	16×31 mm	Ultimate Strength	600 N/mm^2	Weight	123 g/m^2	
Dimensions of Strand	1.25×1.5 mm	Ultimate Strain	58.8×10^{-3}	Volume Fraction	0.535%	
Proof Stress	199 N/mm^2	Proof Strain	1.17×10^{-3}	Tensile Strength	325 N/mm^2	
Proof Strain	9.7×10^{-3}			Elongation	5.5%	
Ultimate Strength	320 N/mm^2					
Ultimate Strain	59.2×10^{-3}					

Table 3. Physical and mechanical properties of polypropylene fibers 300-e3.

Fiber Length	Type / Shape	Absorption	Specific Gravity	Electrical Conductivity	Acid &Salt Resistance	Melt Point	Ignition Point	Thermal Conductivity	Alkali Resistance
Various	Graded / Fibrillated	Nil	0.91	Low	High	162°C (324°F)	593°C (1100°F)	Low	Alkali Proof

Table 4. Ferrocement mortar mix proportions by weight/m^3.

Mix. Designation	Cement (kg)	SF. (kg)	PFA (kg)	Sand (kg)	Water (kg)	Super plasticizer	Fibres (kg)
M	408	68	204	1360	238	6.8	0.9

2.3. Volume fraction of reinforcement (V_r%)

Volume fraction of reinforcement is the total volume of reinforcement per unit volume of ferrocement. For a composite reinforced with meshes with square openings, (V_r) is equally divided into (V_{rt}) and (V_{ri}) for the longitudinal and transverse directions, respectively (Rao and Rao, 1987; Rosenthal and Bljuger, 1985).

2.4. Preparation of test specimens

A special wooden mold, Fig. 4, was designed and manufactured to cast U-shaped ferrocement forms .The ferrocement U-shaped forms were prepared in the following sequence:

1. The wooden mold was assembled and the reinforcing steel mesh was formed in a U-shaped form and the steel bars of 6 mm diameter were tight with steel mesh inside the ferrocement U-shaped forms and placed in the vent of the mold. The constituents of the mortar were mixed and cast in each vent to the required thickness of 25 mm.

2. Wooden pans were placed on top of the cast ferrocement layer and the sides of the ferrocement forms were cast around the wooden pans in the vent of the wooden mold.

3. The ferrocement forms were left for 24 hours in the mold before disassembling the mold. At the end of this step, three U-shaped ferrocement forms are produced. The forms were covered with wet burlap for 28 days.

2.5. Test setup

At the time of testing, the specimen was painted with white paint to facilitate the visual crack detection during testing process. A set of eight "demec" points was placed on one side of the specimen to allow measuring the strain versus load during the test. Demec points were placed as shown in Fig. 5.

The specimen was laid on a universal testing machine of maximum capacity of 100 kN, where the test was conducted under a four-point loads system with a span of 1800 mm. Three dial gauges with an accuracy of 0.01 mm were placed under the test specimen at the center to measure the deflection versus load. Load was applied at 5 kN increments on the specimen exactly at the center. The horizontal distance between each pair of demec points was recorded by using a mechanical strain gauge reader. Concurrently, the beam deflections were determined by recording the dial gauge reading at each load increment. Cracks were traced throughout the sides of the specimen and then marked with red and black markers. The first crack-load of each specimen was recorded. The load was increased until complete failure of the specimen was reached. Fig. 6 shows the test setup.

Fig. 4. U shape wooden mold.

Fig. 5. Demec sets.

Fig. 6. Test setup.

3. Experimental Results and Discussions

The experimental results of the test program and the discussions are presented. Comparisons are conducted between the results of the different test groups to examine the effect of the test parameters under investigation; existence of the permanent ferrocement forms, type of mesh reinforcement. The effects of these parameters on the structural responses of the proposed beams in terms of failure load, mode of failure, first crack load, service load, ductility ratio, and energy absorption were studied extensively. Table 5 presents First crack, serviceability, ultimate loads, ductility ratio and energy absorption properties of all the tested slabs.

Table 5. First crack, serviceability, ultimate loads, ductility ratio and energy absorption properties of all the tested slabs.

Slab No	First crack load (kN)	Service load (kN)	Ultimate Load (kN)	Def. at F.C.L (mm)	Def. at Ult. Load (mm)	Ductility ratio	Energy Absorption (kN·mm)
S1 control	10	10.56	19	16.45	32.15	1.95	393.98
S2 control	15	13.25	23.3	22	41.94	1.91	600.54
S3	15	10.68	19.17	19.11	30.58	1.60	413.8
S4	15	12.43	22	15.2	35.5	2.34	463.3
S5	15	14.19	24.8	17.1	32.2	1.88	509.28
S6	18	16.19	28	18.5	25.9	1.4	587.15
S7	15	9.38	17.1	28.32	34.7	1.23	372.72
S8	15	11.81	21	25.3	38.3	1.51	495.65
S9	15	8.75	16.1	27.36	36.89	1.35	395.87
S10	18	14.31	25	35.1	43.2	1.23	529.6

3.1. Flexural serviceability load

The flexural serviceability load was calculated from the load-deflection curves. It is defined as the load corresponding to deflection equal to the span of the slab (2300 mm) divided by (constant=250) according to The Egyptian Code. Fig. 7 represents the values for the first cracking load, serviceability load and ultimate load for all the tested slabs. Maximum ultimate load reached 28 kN for S6 and minimum ultimate load achieved 19 kN for control slab S1.

3.2. Ductility ratio

The ductility ratio was calculated as the mid span deflection at the ultimate load to that of the first cracking load. Slabs reinforced with expanded metal mesh and welded steel mesh were given higher ductility ratio than control beam. Slabs S9 and S10 were given lower ductility ratio than control slabs. Fig. 8 shows ductility ratios for all tested slabs.

3.3. Energy absorption

The energy absorption was obtained by calculating the area under the load-deflection curve for each slab. Slabs reinforced with expanded steel mesh were achieved higher energy absorption than control slab. Slabs reinforced with welded metal mesh reached higher energy absorption than control slab. Fig. 9 emphasises energy absorption for all tested slabs. Higher ductility and energy absorption properties are very useful for dynamic applications.

3.4. Behaviour of the test specimens

The behaviour of the test specimens in terms of load-deflection relationship, cracking behaviour, and mode of failure is discussed in the following sections.

3.4.1. Load-Deflection relationship

The load-deflection curves of the control specimen (S1 and S2), the specimens incorporating ferrocement forms and reinforced with expanded steel mesh (designations S3 and S4, reinforced welded wire mesh (designations S5 and S6) and those reinforced with Fiberglass mesh (designations S7 and S8). Ferrocement channels (S9 and S10) reinforced expanded steel mesh and steel bars. Figs. 10-14 show load deflection curves for all the test specimens while Fig. 15 emphasises comparison of load deflection curves for all the tested channels.

The load-deflection relationship for the control specimens was linear up to a load of 10-15 kN approximately after which the relation became non-linear. For this group of specimens, the transition from the second to the third stages, as explained before, was not distinct as shown in Fig. 10. At failure, the mid-span deflection reached 37.9 mm, and 44.5 mm for specimens S1 and, S2 respectively. And the ultimate load was 19 and 23.3 for S1 and, S2, respectively. S2 is higher than S1 as a result of the effect of polypropylene fibres employed.

For group B (designations S3 and S4) specimens reinforced with single layer of expanded wire mesh and two layers of expanded steel mesh respectively., The load-deflection relationship was almost linear up to load of about 15 kN and 15 kN for specimens S3 and S4 respectively when the deviation from the linear relation started. Maximum deflection reached 35.5 mm and 36 mm for specimens S3 and S4 respectively (Fig. 11). For group C, when S5 and S6 specimens reinforced with double layers of welded wire mesh and four layers of welded steel mesh respectively. The load-deflection relationship was almost linear up to load of about 15 kN and 18 kN respectively for specimens S5 and S6 respectively when the deviation from the linear relation started as shown in Fig. 12. At failure, the deflection reached 37 mm, 38.7 mm for slabs S5 and S6, respectively.

For group D (designations S7 and S8) specimens reinforced with one layer of fibre glass mesh and two layers of fibre glass mesh respectively, the load-deflection relationship was almost linear up to load of about 15 kN and 15 kN when the deviation from the linear relation started as shown in Fig. 13. At failure, the deflection reached 40.5 mm and 42.6 mm for slabs S7 and S8, respectively. For group E (S9 and S10) specimen reinforced with double layers of expanded steel mesh and one layer expanded steel mesh with skeletal steel bars, the load-deflection relationship was almost linear up to load of about 15 kN and 18 kN respectively when the deviation from the linear relation started as shown in Fig. 14. At failure, the deflection reached 40.9 mm and 47.6 mm, respectively.

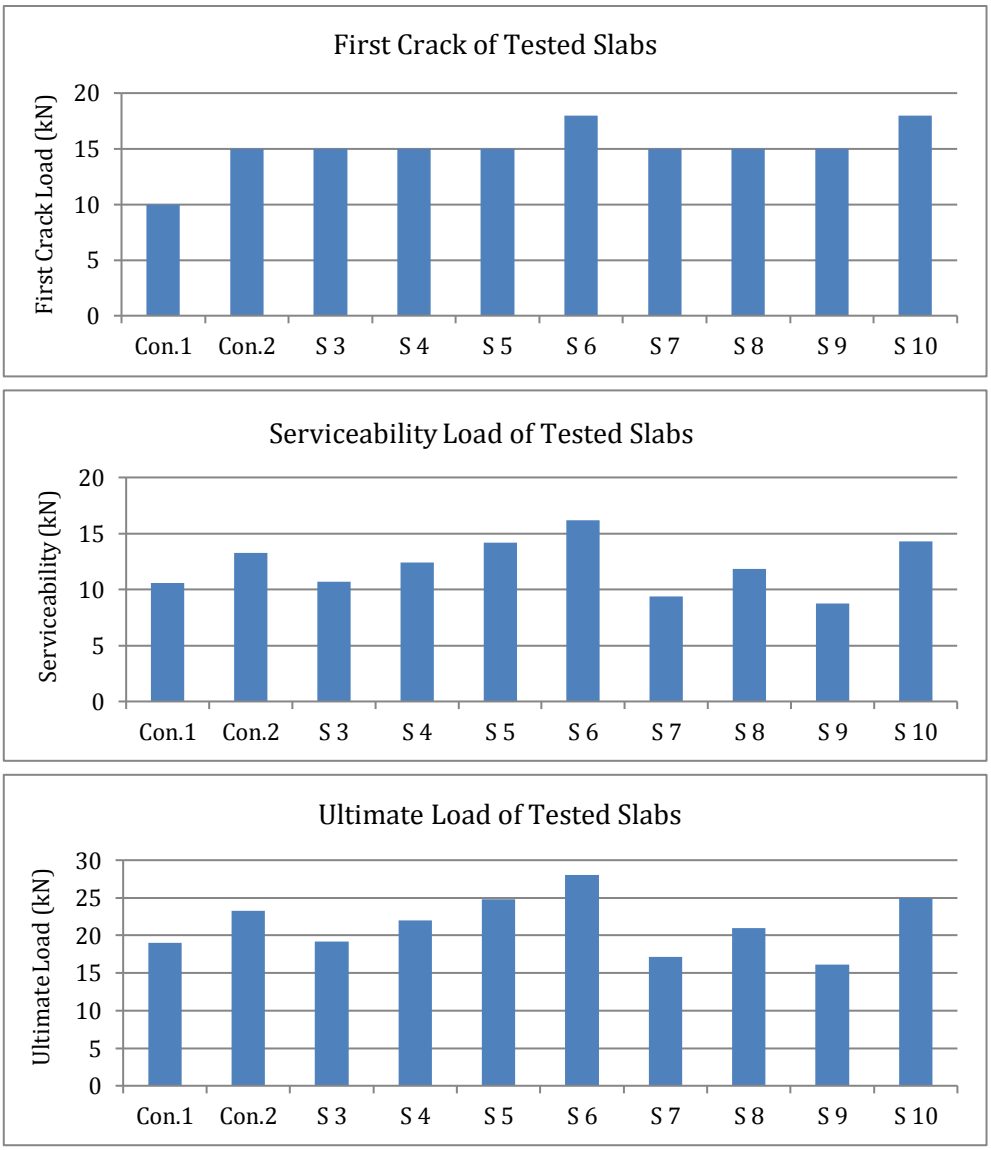

Fig. 7. First crack, serviceability and ultimate loads of all tested slabs.

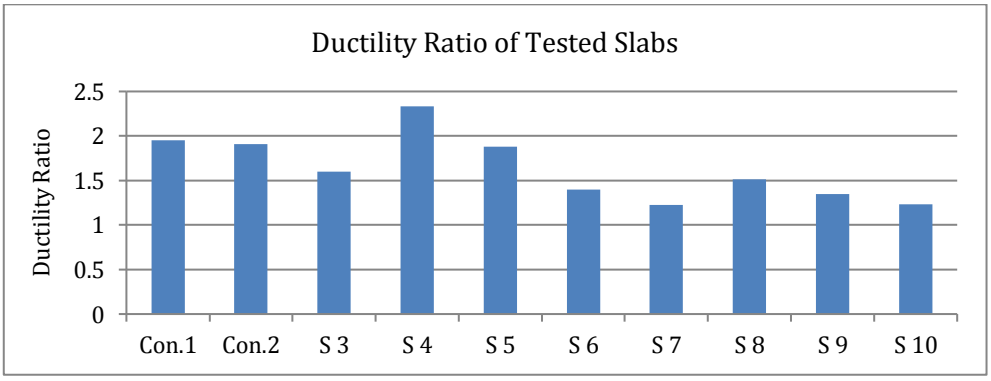

Fig. 8. Ductility ratios for all tested slabs.

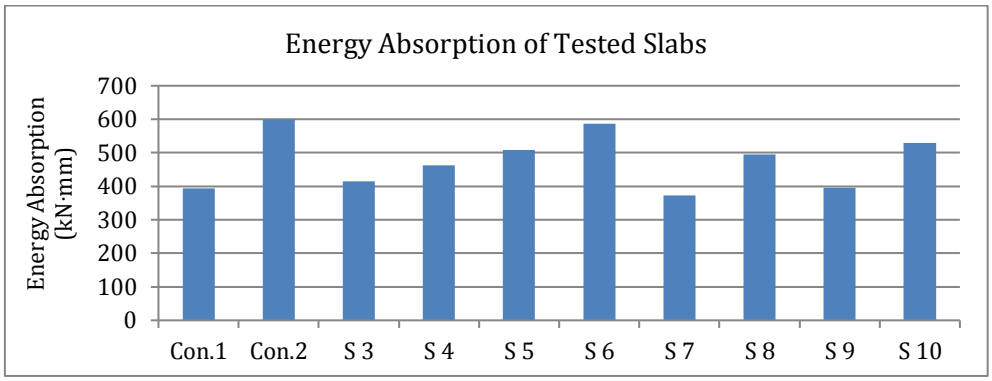

Fig. 9. Energy absorption for all tested slabs.

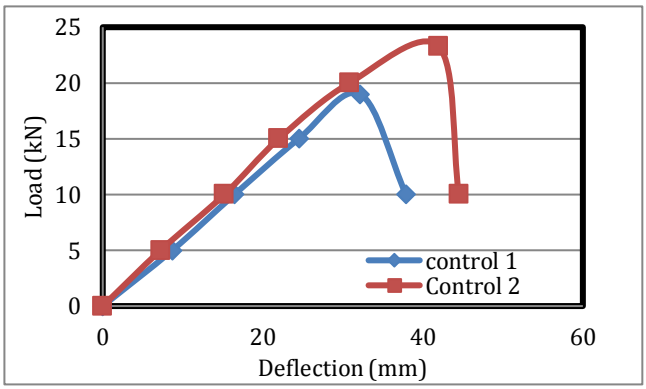

Fig. 10. Load-Deflection curves for group A.

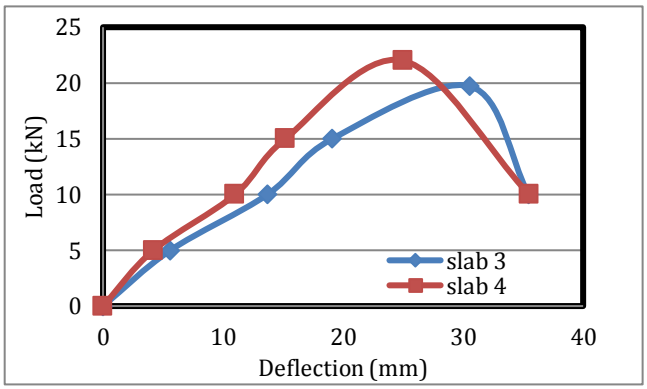

Fig. 11. Load-Deflection curves for group B.

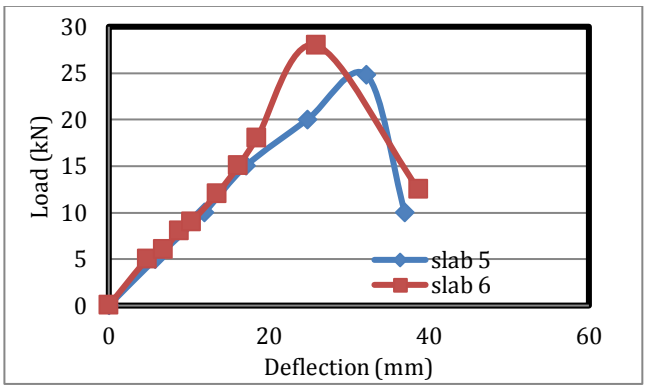

Fig. 12. Load-Deflection curves for group C.

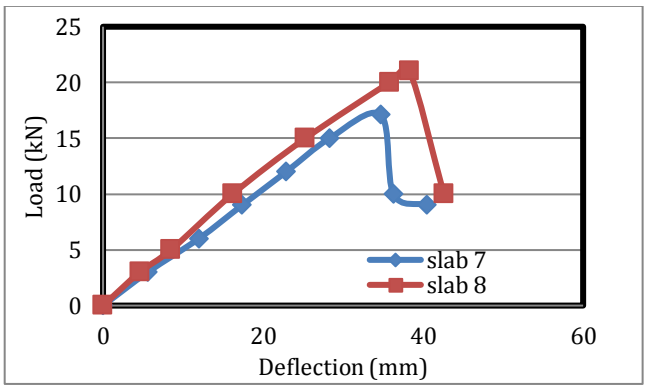

Fig. 13. Load-Deflection curves for group D.

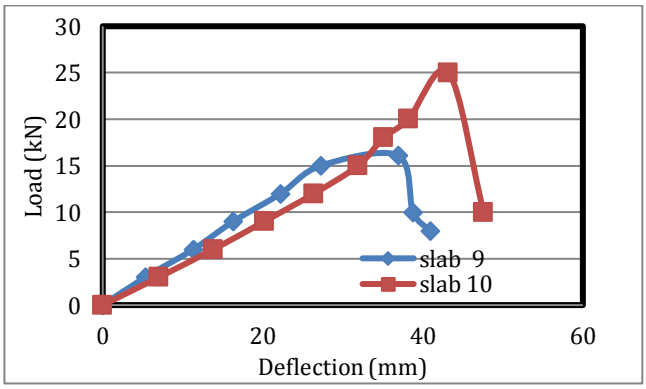

Fig. 14. Load-Deflection curves for group E.

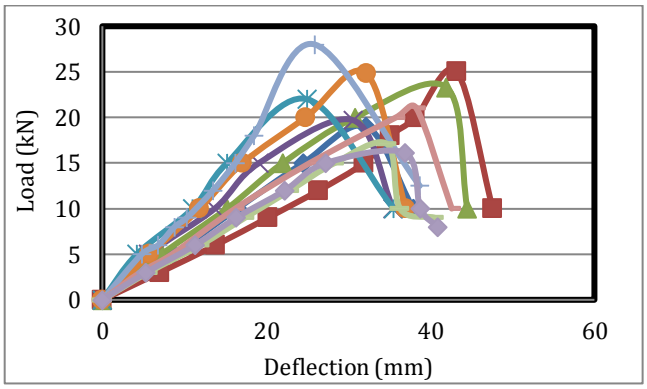

Fig. 15. Load-Deflection curves for all slabs.

3.4.2. Concrete strain

For Control A group specimens, S1 and S2. For slab S1, the compressive strain at the gauge location increased with the increase of the applied load. The maximum compressive strain at this location reached about -0.0038 strain at maximum load 19 kN. The compressive strain at gauge location number 2 followed similar trend. However, the strain at this location was less than that at location number 1 as shown from Fig. 16.

For slab S2, the compressive strain at the gauge location increased with the increase of the applied load. The maximum compressive strain at this location reached about -0.0048 strain at maximum load 23.3 kN. The compressive strain at gauge location number 2 followed similar trend. However, the strain at this location was less than that at location number 1 as shown from Fig. 17. The tensile strains at locations number 3 and 4 increased with the increase of the applied load with the strain at location number 3 being less than that at location number 4. At failure, the tensile strain reading reached 0.00429 strain at location number 4 as shown from Fig. 17.

For group B (S3, S4) specimens reinforced with single layer of expanded wire mesh, the compressive strain at the gauge location (location no. 1) increased almost linearly up to load of 15 kN when deviation from the linear relationship started as shown in Fig. 18. The maximum compressive strain at this location reached about -0.0038 strain at a load of 19.7 kN. The compressive strain at gauge location number 2 followed similar trend. However, the strain at this location was less than that at location number 1. The tensile strains at locations number 3 and 4 increased with the increase of the applied load with the strain at location number 3 being less than that at location number 4. At failure, the tensile strain reading reached 0.004015 strains at location number 4.

For S4, specimens reinforced with double layer of expanded wire mesh, the compressive strain at the gauge location (location no.1) increased almost linearly up to load of 15 kN when deviation from the linear relationship started as shown in Fig. 19. The maximum compressive strain at this location reached about -0.003 strain at a load of 22 kN. The compressive strain at gauge location number 2 followed similar trend. However, the strain at this location was less than that at location number 1. The tensile strains at locations number 3 and 4 increased with the increase of the applied load with the strain at location number 3 being less than that at location number 4. At failure, the tensile strain reading reached 0.001339 strains at location number 4.

For group C (designations S5 and S6) specimens S5 reinforced with two layer of welded wire mesh, the maximum compressive strain at this location reached about -0.002 strain at a load of 24.8 kN. The compressive strain at gauge location number 2 followed similar trend. However, the strain at this location was less than that at location number 1 as shown in Fig. 20. The tensile strains at locations number 3 and 4 increased with the increase of the applied load with the strain at location number 3 being less than that at location number 4. At failure, the tensile strain reading reached 0.002343 strain at location number 4 as shown in Fig. 20.

For specimen S6, reinforced with four layers of welded wire mesh, the compressive strain at the gauge location (location no. 1) increased with the increase of the applied load. The maximum compressive strain at this location reached about -0.0037 strain at load 28 kN. The tensile strains at locations number 3 and 4 increased with the increase of the applied load with the strain at location number 3 being less than that at location number 4. At failure, the tensile strain reading reached 0.0099 strain at location number 4. Fig. 21 shows load strain curves for slab S6.

For group D (designations S7 and S8). Specimens S7 reinforced with single layer of fiberglass mesh, the maximum compressive strain at this location reached about -0.0031 strain at a load of 17.1 kN. The compressive strain at gauge location number 2 followed similar trend. However, the strain at this location was less than that at location number 1. The tensile strains at locations number 3 and 4 increased with the increase of the applied load with the strain at location number 3 being less than that at location number 4. At failure, the tensile strain reading reached 0.004304 strain at location number 4. Fig. 22 shows load strain curves for slab S7.

Specimens S8 reinforced with double layers of fiberglass mesh, the maximum compressive strain at this location reached about -0.0034 strain at a load of 21 kN. The compressive strain at gauge location number 2 followed similar trend. However, the strain at this location was less than that at location number 1. The tensile strains at locations number 3 and 4 increased with the increase of the applied load with the strain at location number 3 being less than that at location number 4. At failure, the tensile strain reading reached 0.00418 strain at location number 4. Fig. 23 shows load strain curves for slab S8.

For group E (designations S9 and S10) Slab S9 reinforced with double layers of expanded steel mesh, the maximum compressive strain at this location reached about -0.00207 strain at a load of 16.1 kN. The compressive strain at gauge location number 2 followed similar trend. However, the strain at this location was less than that at location number 1. The tensile strains at locations number 3 and 4 increased with the increase of the applied load with the strain at location number 3 being less than that at location number 4. At failure, the tensile strain reading reached 0.001532 strains at location number 4. Fig. 24 shows load strain curves for slab S9.

Slab S10 reinforced with one layer of expanded steel mesh and skeletal steel bars. The maximum compressive strain at this location reached about -0.0043 strain at a load of 25 kN. The compressive strain at gauge location number 2 followed similar trend. However, the strain at this location was less than that at location number 1. The tensile strains at locations number 3 and 4 increased with the increase of the applied load with the strain at location number 3 being less than that at location number 4. At failure, the tensile strain reading reached 0.00397 strains at location number 4. Fig. 25 shows load strain curves for slab S9.

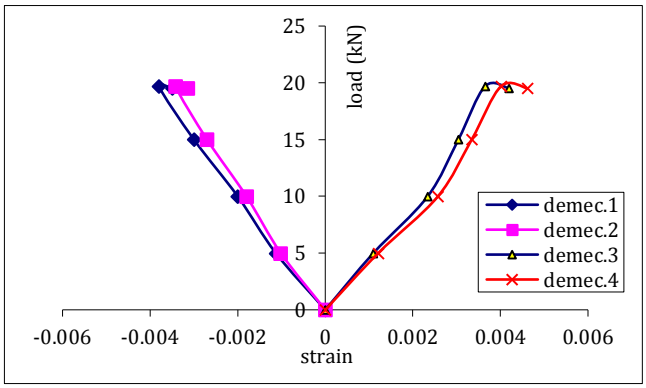

Fig. 16. Load-Strain curve of S1.

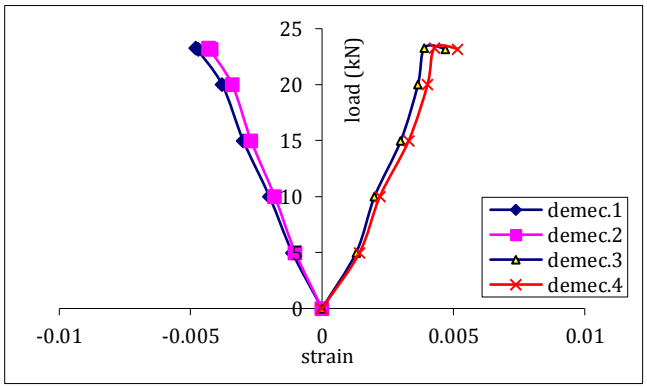

Fig. 17. Load-Strain curve of S2.

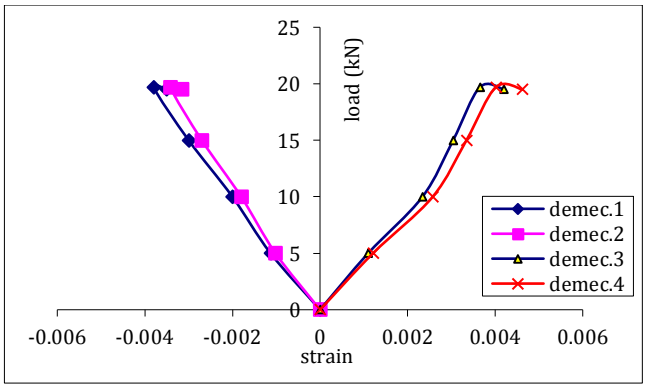

Fig. 18. Load-Strain curve of S3.

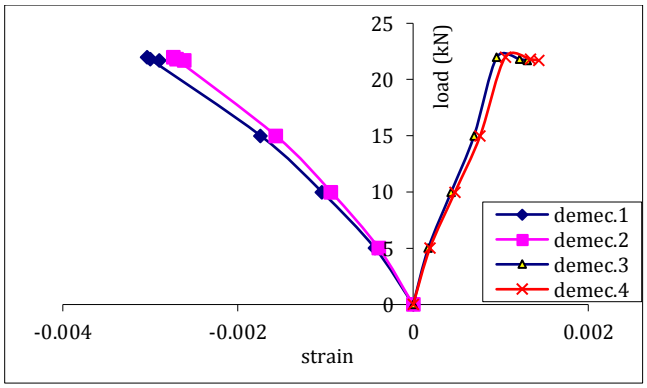

Fig. 19. Load-Strain curve of S4.

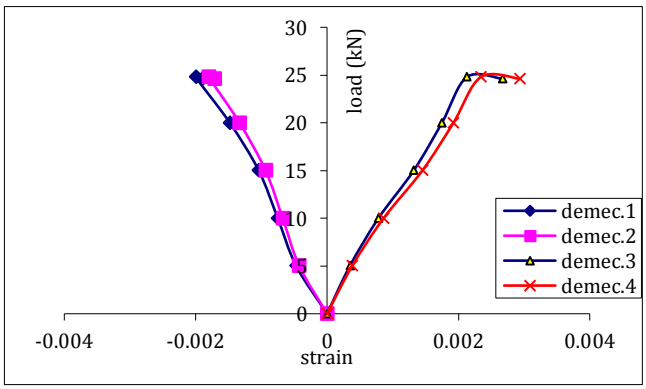

Fig. 20. Load-Strain curve of S5.

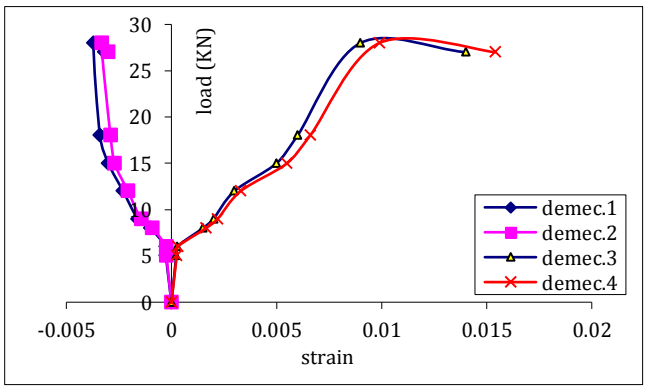

Fig. 21. Load-Strain curve of S6.

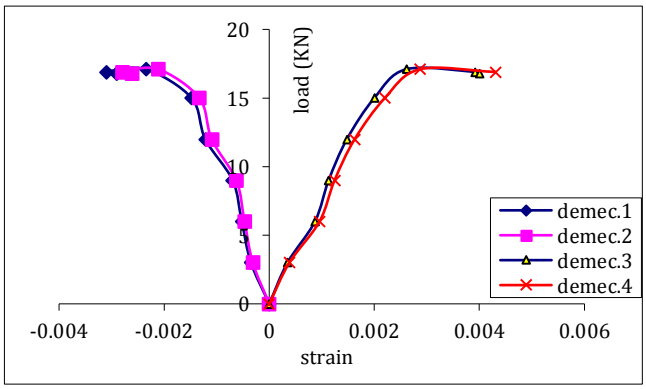

Fig. 22. Load-Strain curve of S7.

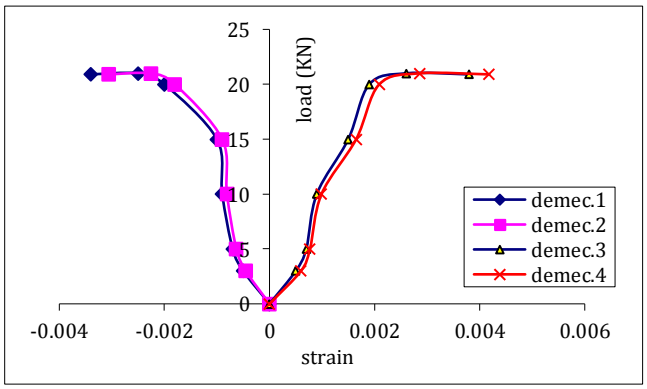

Fig. 23. Load-Strain curve of S8.

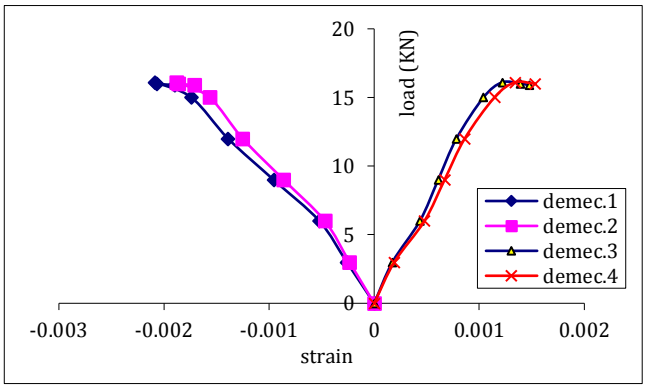

Fig. 24. Load-Strain curve of S9.

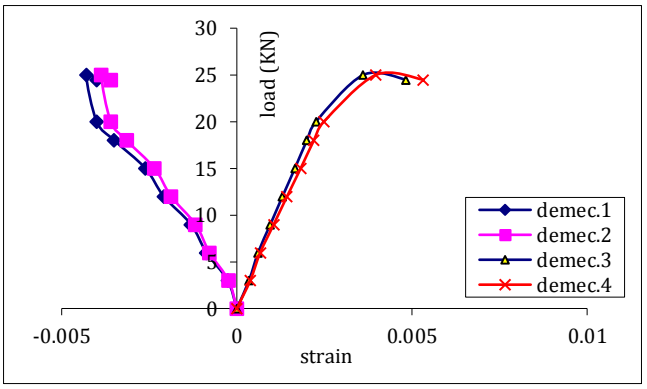

Fig. 25. Load-Strain curve of S10.

3.5. Cracking pattern and mode of failure

3.5.1. Control specimen

Fig. 26 shows the tensile crack, compressive crack and side views of crack patterns of all the tested slabs.

For designation A, flexural crack developed near the mid-span of the specimens of this designation at load of approximately 10 and 15 kN, for slab S1 and S2 respectively. Upon increasing the load, the cracks propagated rapidly upwards and increased in number along the span.

The length and width of the cracks increased with the increase of the applied load. Moreover, diagonal or inclined cracks developed at both ends of the specimen. Failure of the control specimens occurred due to flexure and crushing of the concrete surface at load of 19 kN for S1 and 23.3 kN for S2 as shown in Fig. 26.

3.5.2. Specimens incorporating ferrocement forms reinforced with expanded steel mesh

For designation (B) slabs S3 and S4, it is interesting to note that vertical flexural crack started to develop close to the centre of the span. As the load increased, more cracks started to develop in S3 and S4 and the crack at mid-span started to propagate vertically towards the top surface of the specimen. The crack widths were much less than those of designation A control, this could be attributed to the effect of No. of steel meshes in controlling the crack width. Failure of this type of specimens occurred due to flexural failure as shown in Fig. 26.

3.5.3. Specimens incorporating ferrocement forms reinforced with welded steel mesh

For designation (C) slabs S5 and S6, which reinforced with two and four layers of welded galvanized steel mesh size respectively, it is interesting to note that vertical flexural crack started to develop close to the centre of the span. As the load increased, more cracks started to develop in S5 and S6 and the crack at mid-span started to propagate vertically towards the top surface of the specimen. The crack widths were much less than those of designations A and B. This could be attributed to the effect of No. of steel meshes in controlling the crack width. The flexural crack developed near the mid-span of the specimens of this designation at load of approximately 15 kN and 18 kN for slabs S5 and S6 respectively. With increasing the load, the cracks propagated vertically and new flexural cracks were developed rapidly. As the specimens approached their failure load, the crack started to propagate wider. Failure of this type of specimens occurred due to flexural failure. There is no spalling of concrete cover this is predominant as shown in Fig. 26.

3.5.4. Specimens incorporating ferrocement forms reinforced with fiberglass steel mesh

For designation (D) slabs S7 and S8 which reinforced with one and two layers of fibre glass meshes respectively. It is interesting to note that vertical flexural crack for this type of specimens stared at mid-span and propagated vertically towards the top side of the beam and increased in number along the span. The rate of crack propagation was less than that for the control specimen. Although the crack width was not measured in the test, the visual crack width was less than that of the control specimen. Failure of this type of specimens occurred after crack. Flexural crack developed near the mid-span of the specimens of this designation at load of approximately 15 kN for slabs S7 and S8. Flexural ultimate loads for slabs S7 and S8 reached 17.1 and 21 kN respectively. Fig. 26 shows the cracking pattern of all the tested U shape slabs.

3.5.5. Specimens incorporating ferrocement forms reinforced with fiberglass steel mesh

For designation (D) slabs S7 and S8 which reinforced with one and two layers of fibre glass meshes respectively. It is interesting to note that vertical flexural crack for this type of specimens stared at mid-span and propagated vertically towards the top side of the beam and increased in number along the span. The rate of crack propagation was less than that for the control specimen. Although the crack width was not measured in the test, the visual crack width was less than that of the control specimen. Failure of this type of specimens occurred after crack. Flexural crack developed near the mid-span of the specimens of this designation at load of approximately 15 kN for slabs S7 and S8. Flexural ultimate loads for slabs S7 and S8 reached 17.1 and 21 kN respectively. Fig. 26 shows the cracking pattern of all the tested U shape slabs.

Crack pattern of S1

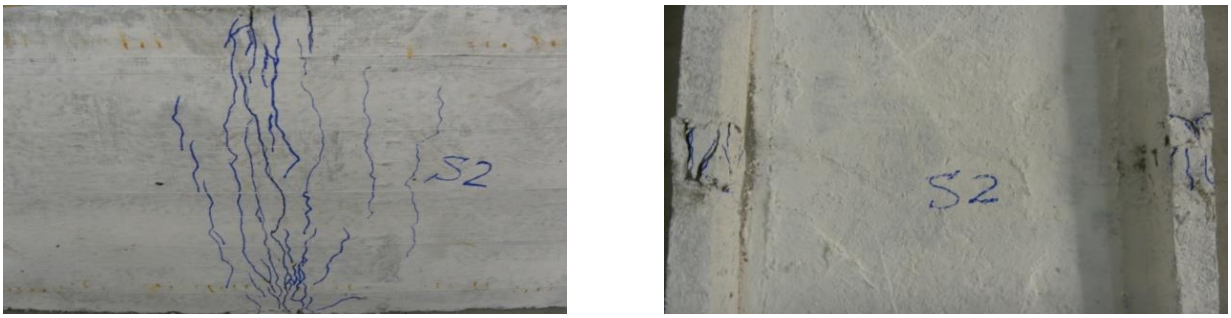

Crack pattern of S2

Crack pattern of S3

Crack pattern of S4

Crack pattern of S5

Crack pattern of S6

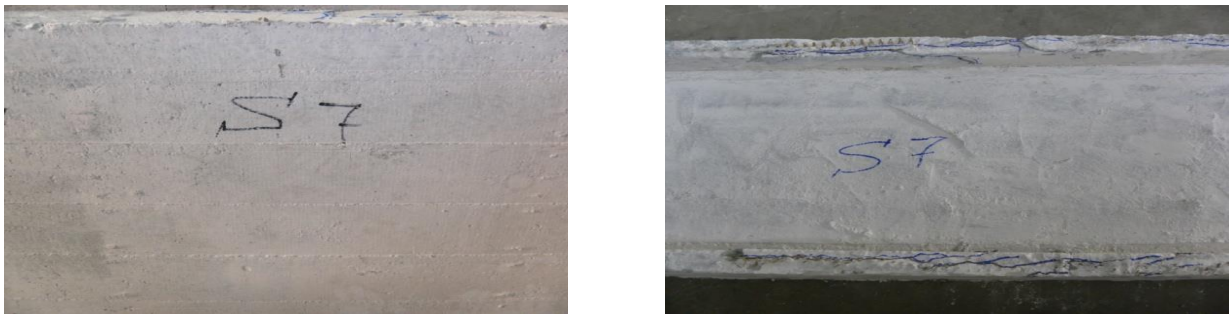

Crack pattern of S7

Crack pattern of S8

Crack pattern of S9

Crack pattern of S10

Fig. 26. Crack patterns of all tested slabs.

3.6. Effect of the test parameters

The effect of the test parameter is investigated from the experimental results of the test specimens and is discussed in the following sections. The effects of these parameters were studied on the structural responses of the test U shape slabs in terms of first crack load, service load, and failure load, mode of failure, ductility ratio, and energy absorption.

The load-deflection relationship for the control specimens was linear up to a load of approximately 15 kN approximately, when the first crack was observed, after which the relation became nonlinearly. Beyond load of about 17 kN the mid-span deflection increased with much higher rate indicating yielding of the steel reinforcement. At failure, the mid-span deflection reached 35 mm.

3.6.1. Effect of the existence of synthetic fibres in the mortar mix

The effect of the existence of the synthetic fibres in the mix of the ferrocement mortar on the behaviour of the test specimens is studied by comparing the results of the same specimens containing the fibres in the mix with the corresponding ones without the fibres for series A. and for all groups with others.

The behaviour of the specimens without synthetic fibres was considered as the base for this comparison, the existence of the synthetic fibres in the mortar mix resulted in an increase in the first crack load, serviceability load, ultimate load, and energy absorption. However, it resulted in a decrease in the ductility ratio. Fig. 15 shows the comparison between the load deflection curves for all test specimens.

The existence of the synthetic fibres resulted in retarding the occurrence of the first crack and better crack distribution in the ferrocement U-shaped slabs. This led to a higher stiffness of the test specimen and consequently less deflection at the corresponding load levels as shown in Figs. 11-14. The figures show that the specimens with fibre had a higher deflection at failure as a result of the attained higher ultimate load. However, the ratio of the deflection at ultimate load to that at the first cracking load was lower for the specimens with fibres in comparison to those without fibres which lead to the observed reduction of the ductility ratio as defined in this research.

3.6.2. Effect of the type of the mesh inside the U shape slabs

The effect of reinforcing steel mesh type is studied by comparing the results of groups reinforced with expanded wire mesh with that reinforced with welded steel mesh and fibreglass mesh. The behaviour of expanded wire mesh group was considered as the base for comparison for both single and double layers.

Samples reinforced with welded wire mesh achieved higher first crack load, ultimate load, serviceability load and energy absorption with respect to steel bars and the number of steel mesh.

It is worth mentioning that the ductility of slabs reinforced with expanded wire mesh is higher than that of beams reinforced with welded wire mesh. This is expected since the specimens reinforced with expanded steel mesh had slightly higher volume fraction, 0.04% and 0.231%. However, the proof stress for the expanded steel mesh was much lower than that for the welded wire mesh, 199 N/mm^2 as compared to 400N/mm^2.

3.6.3. Effect of the number of reinforcing steel mesh layers

The effect of the number of reinforcing steel mesh layers is investigated by comparing the results of groups reinforced with single and double layers for both steel mesh types investigated in this research. Doubling the steel mesh layers at the bottom of the specimens resulted in a higher first crack load, serviceability load, ultimate load, and energy absorption. However, the maximum deflection at ultimate load decreased as a result of increasing the specimen's stiffness also the ductility ratio decreased due to the increase of the volume fraction.

The enhancement in mechanical properties due to increasing the number of steel mesh layers for welded wire mesh was much higher than that of expanded wire mesh for the first crack load, ultimate load, and serviceability load and energy absorption. However, the enhancement in reduction in the ductility ratio was almost the same for both types of steel mesh.

4. Conclusions

The results also demonstrated that the presence of fibres in the mix improved the slab's overall performance. Within the scope, parameters, experimental investigation considered in this research and based on the test results and observations of the experimental investigation; the following conclusions and recommendations may be drawn as follows:

- Employing welded galvanized steel mesh gave the highest results compared to all tested U shape tested slabs.
- Using polypropylene fibres in mortar mix increase in the first crack load, serviceability load, ultimate load, and energy absorption, higher stiffness However, it resulted in a decrease in the ductility ratio, less deflection at the corresponding load levels.
- Welded galvanized wire mesh achieved higher first crack load, serviceability load, ultimate load and energy absorption in comparison to reinforce with expanded and glass fibre meshes..
- Using (two-four) layers of welded galvanized steel mesh in reinforcing ferrocement U shaped slabs, improve the energy absorption than obtained when using skeletal steel bars.
- Using U-shaped welded steel mesh with mild steel bars in reinforcing ferrocement slabs higher energy absorption than of using mild steel bars only. However the U-shaped showed less ductility ratio.
- Using four steel bars with one layer expanded metal mesh improve ductility ratio and energy absorption compared with using two-layer expanded metal mesh only.

- Increasing the number of the steel mesh layers in the ferrocement forms increases the first crack load, service load, ultimate load, and energy absorption decreases the ductility ratio of the U shaped slab.
- Using welded steel wire mesh reinforcement decreased the ductility ratio compared to that reinforced with glass fibre mesh and expanded steel mesh.
- The ductility ratio reduced. The percentage of reduction depends on the type and number of steel mesh layers in the ferrocement U shaped forms.

REFERENCES

Abdel Tawab A (2006). Development of Permanent Formwork for Beams Using Ferrocement Laminates. *Ph.D thesis*, Menoufia University, Shebin El-Kom, Egypt.

Abdul Kadir MR, Jaafar MSH (1993). Ferrocement in situ permanent formwork. *Journal of Ferrocement*, 23(2), 125-133.

Abdul Kadir MR, Abdul Samad AA, Che Muda Z, Ali AAA (1997). Flexural Behavior of Composite Beam with ferrocement Permanent Formwork. *Journal of Ferrocement*, 27, 209 - 214.

ACI 549-1R-88 (1998). Guide for the Design, Construction, and Repair of Ferrocement, Manual of Concrete Practice. American Concrete Institute, Farmington Hill, Michigan, USA.

Ayoub STAE (2005). Flexural Behavior of High Strength Concrete Beams Reinforced with Advanced Composite Materials. *M.Sc thesis*, Menoufia University, Shebin El-Kom, Egypt.

Channi AS (2009). Effect of Percentage of Reinforcement on Beams Retrofitted with Ferrocement Jacketing. *M.Sc thesis,* Thapar University, Patiala, India.

El-Halfawy EMAF (2003). Flexural Behavior of Ferrocement Deck Bridges. *M.Sc thesis*, Menoufia University, Shebin El-Kom, Egypt.

ElMohimen HMRA (2005). Structural Behaviour of Ribbed Ferrocement Plate. *B.Sc thesis*, Menoufia University, Shebin El-Kom, Egypt.

El-Sakhawy YME (2007). Structural Behaviour of Ferrocement Roof Elements. *M.Sc thesis*, Menoufia University, Shebin El-Kom, Egypt.

Fahmy EH, Shaheen YBI (1991). Strengthening and repairing of reinforced concrete tanks. *Fourth Arab Structural Engineering Conference*, United Arab Emirates, 18-21.

Fahmy EH, Shaheen YBI, El-Dessouki WM (1995). Application of ferrocement for construction of radial gates. *Journal of Ferrocement,* 25(2), 115-121.

Fahmy EH, Shaheen YBI, Korany YS (1997a). Repairing reinforced concrete beams by ferrocement. *Journal of Ferrocement*, 27(1), 19-32.

Fahmy EH, Shaheen YBI, Korany YS (1997b). Use of ferrocement laminates for repairing reinforced concrete slabs. *Journal of Ferrocement*, 27(3), 219-232.

Fahmy EH, Shaheen YBI, Korany YS (1999). Repairing reinforced concrete columns using ferrocement laminates. *Journal of Ferrocement*, 29(2), 115-124.

Fahmy EH, Shaheen YBI, Abou Zeid MN (2004). Development of ferrocement panels for floor and wall construction. *5th Structural Specialty Conference of the Canadian Society for Civil Engineering*, Canada.

Housing and Building Research Center (HBRC) (2001). The Egyptian Code for Design and Construction of Concrete Structures, Cairo, Egypt.

Mansur MA, Paramasivam P (1990). Ferrocement short columns under axial and eccentric compression. *ACI Structural Journal*, 87(5), 523-529.

Mays GC, Barnes RA (1995). Ferrocement permanent formwork as protection to reinforced concrete. *Journal of Ferrocem*ent, 25(4), 331-345.

Naaman AE, Shah SP (1971). Tensile tests of ferrocement. *ACI Journal*, 68(9), 693-698.

Rajagoplan K, Parameswaran VS (1975). Analysis of ferrocement beams. *Journal of Structural Engineering*, 2(4), 155-164.

Ramesht MH, Vickridge I (1996). A computer program for the analysis of ferrocement in flexure. *Journal of Ferrocement*, 26(1), 21- 31.

Rao PK, Rao VJ (1987). Development and application of composite precast ferrocement and concrete roofing/flooring system. *Proceedings of the First International Conference on Structural Science and Engineering*, India.

Rosenthal I, Bljuger F (1985). Bending behavior of ferrocement – reinforced concrete composite. *Journal of Ferrocement*, 15(1), 15-24.

Sandowicz M, Grabowski J (1985). Application of ferrocement channel elements to housing. *Proceedings of the Second International Symposium on Ferrocement,* International Ferrocement Information Center, Bangkok. 493- 505.

Shaheen YBI, Eltaly B, Henish A (2014). Experimental and FE simulations of ferrocement domes reinforced with composite materials. *Concrete Research Letters*, 5(4), 837-887.

Shaheen YBI, Mahmoud AM, Refat HM (2016). Structural performance of ribbed ferrocement plates reinforced with composite materials. *Structural and Engineering Mechanics*, 60(4), 567-594.

Singh G, Bennett EW, Fakhri NA (1988). Influence of reinforcement on fatigue of ferrocement. *The International Journal of Cement Composites and Lightweight Concrete*, 8(3), 151-164.

Sutherland WM (1972). Ferrocement Boats: Service Experience in New Zealand. *FAO Seminar on the Design and Construction of Ferrocement Fishing Vessels*, Wellington, 14 (Also, Fishing News, West Byfleet, Surrey).

Swamy RN, Abboud MI (1988). Application of ferrocement concept to low cost lightweight concrete sandwich panels. *Journal of Ferrocement*, 18(3), 285-292.

Tomar A (2006). Retrofitting of Shear Deficient RC Beams using Ferrocement Laminates. *M.Sc thesis,* Thapar Institute of Engineering and Technology (Deemed University), Patiala, India.

Wrigley RG (2001). Permanent Formwork in Construction. Construction Industry Research & Information Association (CIRIA), London.